Unsteady flow in a branch

By V. O'BRIEN, L. W. EHRLICH AND M. H. FRIEDMAN

Applied Physics Laboratory, The Johns Hopkins University,
Laurel, Maryland 20810

This study was motivated by the focal tendency of atherosclerotic plaque to appear near arterial junctions. A two-dimensional bifurcation was selected to provide preliminary information on branch flow dynamics. Superseding previous steady flow estimates in similar branches, digital solutions for two flux waves have been obtained to reveal temporal and spatial distributions of shear and separation in pulsatile flow. Marked differences from steady flow are illustrated as well as variation due to flux-wave shape.

1. Introduction

Branching flows occur in many situations and this particular theoretical study of unsteady flow in a symmetric branch was motivated by medical research into arteriosclerosis. It is now generally recognized that there are three factors in the problem of developing atherosclerosis in man's large elastic arteries: (i) the vessel wall, especially injury to the endothelium, (ii) the blood, including the lipids within the plasma, and (iii) the hydrodynamics of the blood flow (Mustard *et al.* 1964; Constantinides 1965; Texon, Imparato & Helpern 1965; Fry 1968; Haust 1971). Lacking a clear demonstration of all relevant physical and biological parameters, it is difficult to decide which of the factors is most important, for they are probably mutually coupled. However, the 'focal' tendency of the early plaque to be found near arterial branches, such as the aortic bifurcation (figure 1*a*), suggests a major role for haemodynamics in the localization (Downie, Mustard & Rowsell 1963; Geissinger, Mustard & Rowsell 1962; Murphy *et al.* 1962; Texon, Imparato & Lord 1960; Caro, Fitz-Gerald & Schroter 1969; Middleman 1972). Because the problem of predicting and verifying haemodynamic flow in arterial branches is one of considerable difficulty, a simple, rather idealized branching model was selected for preliminary investigation of unsteady flow dynamics by appropriate numerical techniques.

The simulation of pulsatile incompressible flow within the rigid impermeable two-dimensional model of a symmetric bifurcation shown in figure 1 (*b*) (i.e. a crude analogue of the junction of the abdominal aorta and the iliac arteries; see figure 1(*a*)) reveals unsuspected details of the space- and time-dependent distribution of flow properties near the corner *C* and the divider tip *D*. The flow picture differs from previous steady channel branch calculations (Lynn, Fox & Ross 1972; Cheng & Fijas 1972) or impulsive flow (Hung & Naff 1969). None of these publications were validated but the physical accuracy of our simulation
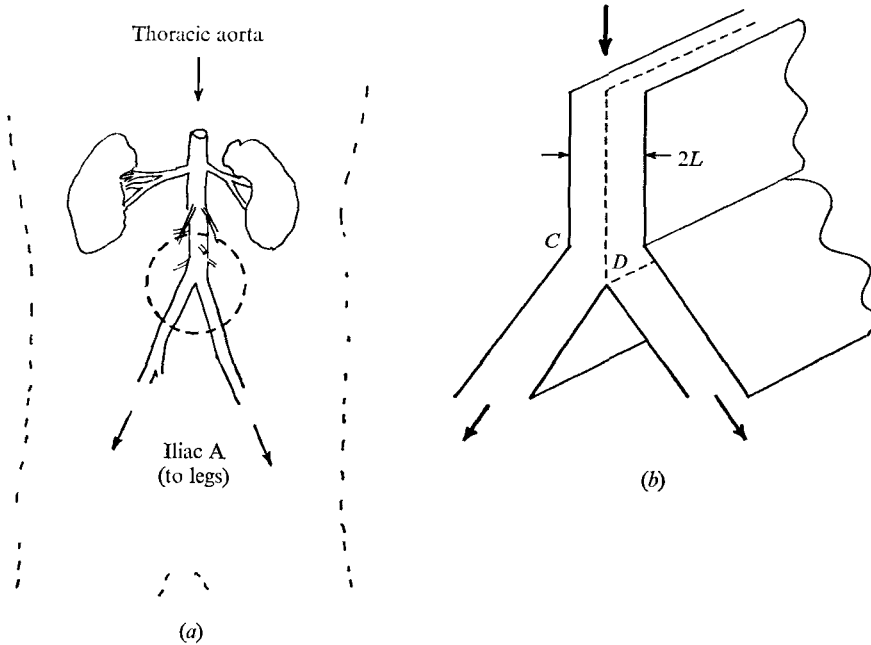
FIGURE 1. Aortic bifurcation model. (*a*) Anatomy of abdominal aorta;
aortic bifurcation circled. (*b*) Two-dimensional model (symmetric).

model has been checked against experimental measurements by laser veloci-
metry in a water channel (Bargeron, Mark & Friedman 1975).

This report provides insight into important time-dependent aspects of a
branch flow. It is obvious that one will not be able to understand fully haemo-
dynamics or its quantitative effect on atherogenesis near branch junctions with-
out allowing for the unsteadiness of the flow field (see Friedman, O'Brien &
Ehrlich 1975). Numerical questions peripherally related to the physics are
considered separately in the appendix. Only samples of our results with the fully
developed input flow will be given, although others have been used and the
system can use any measured inflow. Deficiencies of the simple model for arterial
branches are pointed out in the discussion section (§5). However, a focal tendency
to have the major differences from inflow and outflow located close within the
junction is clearly indicated. Advantages of the numerical method and extension
towards more realistic blood flow models are also discussed. The results could
have application to other branch flows, e.g. corrosion in branching pipes during
chemical processing.

2. Setting the problem

It will be assumed that the flowing fluid can be modelled as a Newtonian
viscous fluid. In principle, every incompressible viscous flow can be determined
from the governing continuity and momentum equations with physically
reasonable boundary conditions. Unfortunately, the momentum equation is
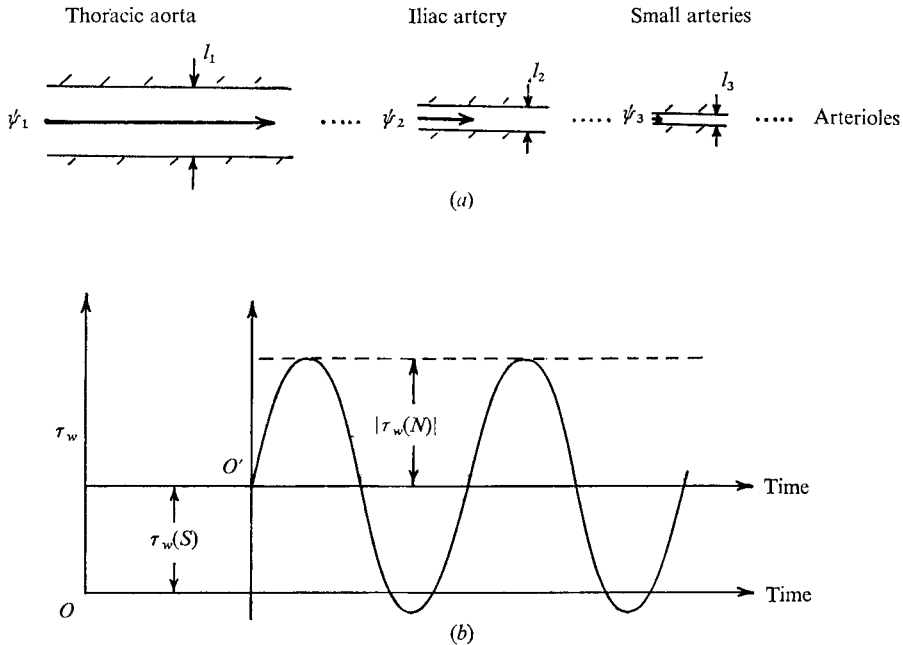
FIGURE 2. One-dimensional pulsatile flow in straight rigid conduits. (a) Anatomy (after Spencer & Denison 1963). (b) Theoretical parallel flow: τ_w is wall stress.

nonlinear and analytically intractable except for special cases. One special class is parallel flow in straight conduits of constant cross-section. Estimates of wall shear for levels of the arterial tree (figure 2) have been made by Whitmore (1968) using the steady flow cylindrical model, where it is predicted that the mean wall shearing rate increases monotonically to a maximum in the capillaries.

If only long straight conduits were involved the theoretical inclusion of fluctuations along with the steady parallel flow component could be achieved analytically, or it could be calculated numerically; see Clark & Robertson (1971). Parallel viscous flow solutions for sinusoidal flux, including a wall shearing stress $\tau_w(N)$, are known theoretically: for round tubes see Grace (1928) and Sexl (1930); for elliptic cylinders see Khamrui (1957); for plane channels see Rott (1964); and for rectangular ducts see O'Brien (1975). Many details have been confirmed experimentally. The wall stress depends on a 'Stokes number' $N = (\pi l^2/\nu T)^{\frac{1}{2}}$ for any given flux oscillation amplitude $|\psi_N|$, where T is the period, ν is the fluid kinematic viscosity and l is a characteristic length. By linear superposition, a steady Poiseuille flow and a sinusoidal fluctuation may be added for all Reynolds numbers Re; fluctuations of other frequencies sum as readily. The peak shearing stress can considerably exceed the mean in these fully developed flows, rising with N (see figure 2(b)).

Without the simplification of parallel flow, nonlinearity comes into play, so that numerical approximate solutions are more practical. A full three-dimensional time-dependent branch problem with any reasonable space resolution would tax the limits of our computer capacity and calculation budget.
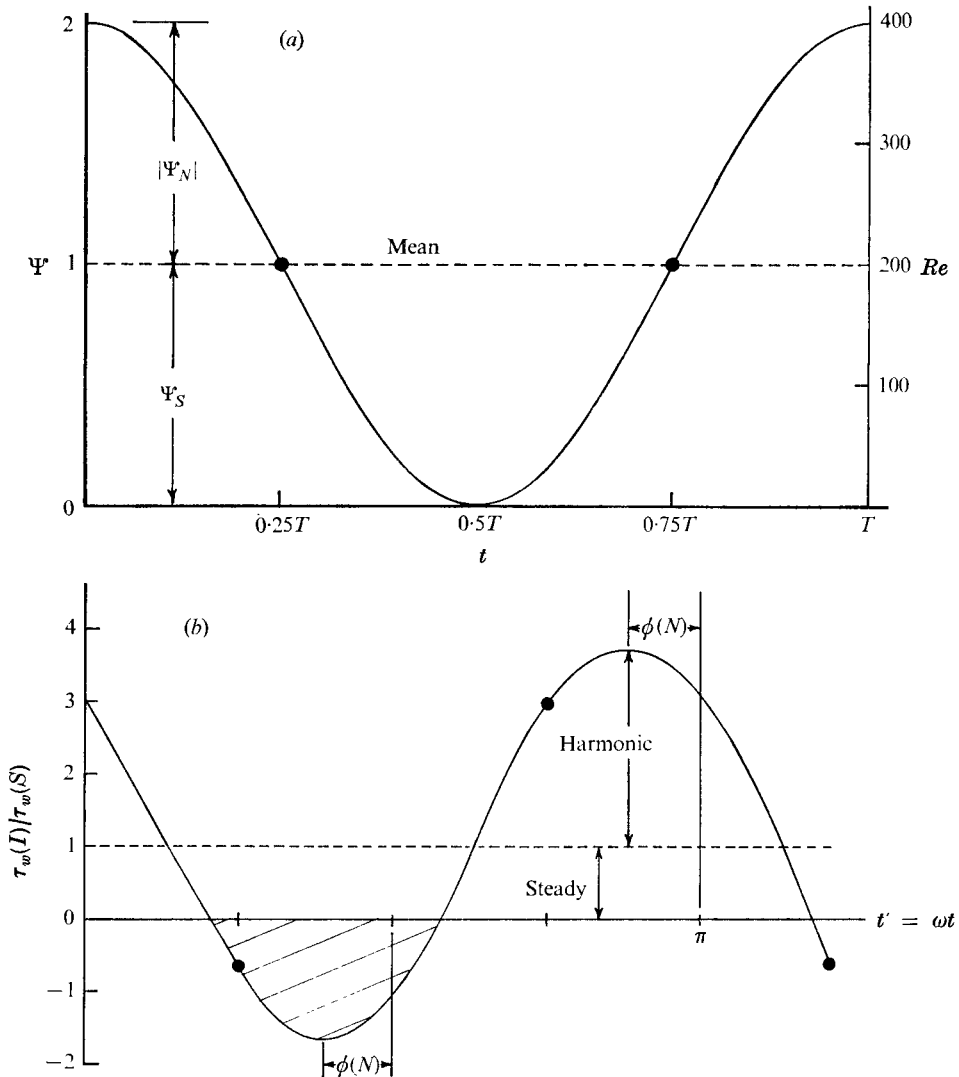
Figure 3. Simple pulsatile flow through a branch. (a) Simple pulsatile flow (definition): Ψ is normalized flux per unit depth, Re is instantaneous Reynolds number. (b) Time-dependent inlet wall stress for pulsatile flow. $N = (\pi/\nu T)^{\frac{1}{2}} 2L = 10$.

Instead, an ideal rigid two-dimensional simulation of the branch geometry was used in the interest of economy, with the knowledge that the result must be carefully interpreted as a partial picture of the flow situation in the three-dimensional orthogonal symmetry plane defined by the geometry of the branch.

First, for convenience, we consider 'a simple pulsatile flow'; see figure 3(a). This is the sum of a steady flux and a single harmonic flux of equal magnitude. The corresponding instantaneous input channel Reynolds number Re used in the calculation is also shown. The Reynolds number governs the influence of the (nonlinear) convective term relative to the viscous diffusion term in the Navier–Stokes equation. It reaches a peak $\hat{Re}$ of 400 (based on the total input channel

width $2L$), where $\hat{Re} = Re(N) + Re(S) = 2\,Re(S)$. The steady Reynolds number $Re(S)$ and fluctuation Reynolds number $Re(N)$ are defined for the two-dimensional flow as

$$Re(S) \equiv \langle U_s \rangle 2L\rho\mu^{-1} \quad \text{(steady)},$$

$$Re(N) \equiv |\langle U_N \rangle| 2L\rho\mu^{-1} \quad \text{(fluctuating)},$$

where $\langle U \rangle$ is the space-mean or average velocity across the input channel and the dimensional quantities μ, ρ and ν are the conventional ones. The channel 'Stokes number' $N \equiv (2L^2\omega/\nu)^{\frac{1}{2}}$, where $\omega = T/2\pi$ is the angular frequency of pulsation. In the figure Ψ is the flux per unit depth normalized with respect to $2L\langle U_s \rangle$. The flux is non-negative throughout the cycle.

The parallel channel input is assumed to be fully developed flow, whose analytic solution as a function of N is known (Rott 1964) and has been verified (O'Brien & Logan 1966). The pulsatile input flow has maximum and minimum limits of total wall shear $\tau_w(S) \pm \tau_w(N)$, conveniently normalized by the mean (i.e. steady) parallel wall shear to remove the dimensionality (figure 3(b)). There is a phase shift $\phi(N)$. Note that, because $|\tau_w(N)| > \tau_w(S)$ for all $N > 0$, there is a time interval of negative shear, which corresponds to periodic flow reversal *along the wall* even though the net flux is never negative (figure 3a). The negative wall shear occupies a greater portion of the cycle as $N \to \infty$.

When more complicated flux waves pass through the Y branch the flow cannot be obtained by Fourier synthesis; owing to nonlinearity every flux wave is an individual problem. A realistic arterial flux-wave shape, obtained *in vivo*, has also been used for a pulsatile branch flow calculation.

3. Theoretical method

The coupled equations for the stream function $\Psi(X, Y, t')$ (normalized flux per unit depth) and vorticity $\Omega(X, Y, t')$ (magnitude of the curl of the normalized velocity vector) are

$$\frac{N^2}{2}\frac{\partial\Omega}{\partial t'} - \frac{Re(S)}{2}[\Psi_X\Omega_Y - \Psi_Y\Omega_X] = \nabla^2\Omega, \tag{1}$$

$$\nabla^2\Psi = -\Omega, \tag{2}$$

where $X = x/L$, $Y = y/L$ and $t' = \omega t = 2\pi t T^{-1}$, where T is the period of fluctuation. Advantage has been taken of the assumed symmetry of flow within the symmetrical branch (figure 4). The velocity components are normalized by $\langle U_s \rangle$:

$$U' \equiv U/\langle U_s \rangle = \partial\Psi/\partial Y, \quad V' \equiv V/\langle U_s \rangle = -\partial\Psi/\partial X.$$

No slip is allowed along the horizontal and sloping impermeable walls (figure 4) so $\Psi(1)$ is a function of t' only and $\partial\Psi(1)/\partial n = 0$ (n is the outward normal direction). On the plane of symmetry ($Y = 0$), $\Omega(X, 0, t') = \Psi(X, 0, t') = 0$. At the inlet the simple pulsatile $\Psi(Y, t')$ and $\Omega(Y, t')$ are known from the analytic solutions. At the outlet the first derivatives of Ψ and Ω along the p (parallel to daughter wall) direction vanish (flow parallel to walls).

The angle of the bifurcation is $90°$. The ratio of the areas of the daughter and inlet channels is $\alpha = 0.8$. Note that the boundary conditions on the walls are

$$\frac{N^2}{2}\frac{\partial\Omega}{\partial t'} - \frac{Re(S)}{2}\,(\Psi_X\,\Omega_Y - \Psi_Y\,\Omega_X) = \nabla^2\Omega$$
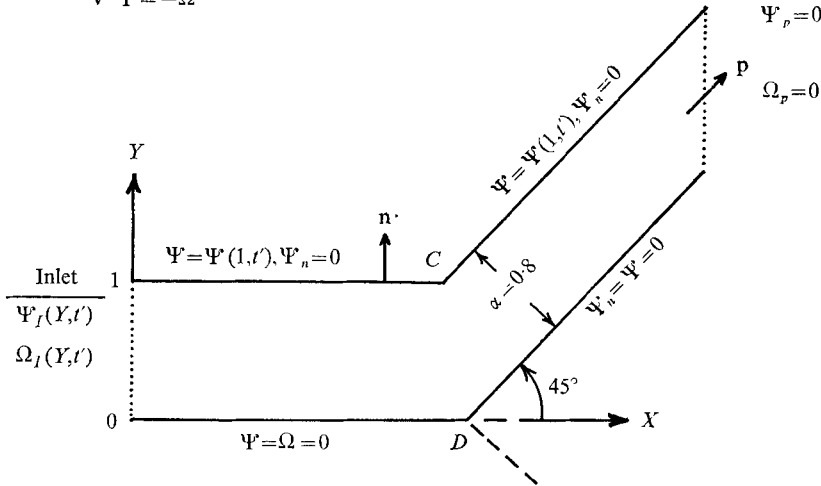
$$\nabla^2\Psi = -\Omega$$

FIGURE 4. Non-dimensional equations and boundary conditions for the calculation.

stated in terms of Ψ (figure 4). Boundary conditions on Ω are needed to solve (1). Applying the fact that the derivatives of Ψ tangential to the boundary vanish, $\Omega = -\Psi_{nn}$ on a solid boundary, where n is a well-defined normal on all the straight sections of the walls. No normal exists for a mathematically sharp corner at C, but all physically smooth corners have a normal everywhere. So an approximation to the local normal at C was obtained by averaging the normals on the two walls approaching the corner. On the basis of previous experience with coupled Ψ, Ω equations (Ehrlich 1971 a,b, 1973 a,b), a two-point second-order $[O(h^2)]$ approximation to Ψ_{nn} was used, where h is the spacing of the finite-difference mesh. See Ehrlich (1974) for details. The nonlinear equation (1) was solved on an IBM 360/91 by explicit marching. There were restrictions on the time step for stability. Numerical analysts may be interested in the discussion of accuracy given in the appendix.

The Poisson equation (2) is linear and could be solved iteratively. However, the method of Hockney (1965), incorporating modifications suggested by George (1970) and Buzbee *et al.* (1971) for non-rectangular regions, allowed efficient direct solution at every time step once $\Omega(X, Y)$ had been evaluated. Other parallel entrance velocity conditions were also used, including steady flow alone. The branch area ratio α was also varied (see Friedman *et al.*).

4. Results of numerical experiments

Simple pulsatile flow

Once the program successfully generates the nonlinear solution (as a function of x, y, t) all information regarding flow dynamics is available. This includes velocity components, wall shear, vorticity, instantaneous streamlines, pressure
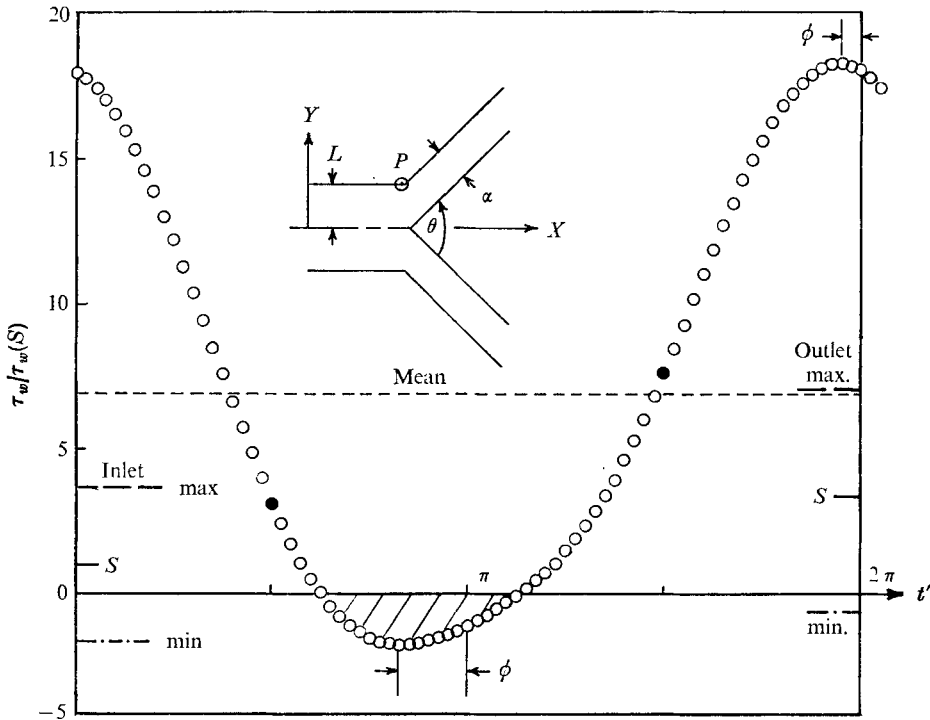
FIGURE 5. Calculated relative wall stress at a point P $(X = 1.875)$ just before the corner C $(\hat{Re} = 400, N = 10, \alpha = 0.8)$.

gradients, etc. The difficulty arises in deciding which of these quantities is most meaningful for appreciating the branch flow (or understanding its relationship to arteriosclerosis etiology). For example, the calculated periodic variation of wall shearing stress at a single point P just before the corner of the branch is shown in figure 5, normalized by the mean inlet wall shear $\bar{\tau}_w(I)$. Note that the mean stress $\bar{\tau}_w$ at this location exceeds both the inlet and outlet mean values. Therefore it is doubtful that the mean shear in the human arterial tree increases monotonically to a maximum in the capillaries (Whitmore).

Flow velocity components display the gross time variation of the simple pulsatile flow field. The appropriate numerical derivatives of $\Psi(X, Y, t')$ are fed into an IBM 2250 graphics display processor and instantaneous velocity vectors are presented on the oscillograph output as directed lines from the mesh points. Figures 6 (a)–(d) show the vector field at intervals during the cycle. The horizontal line just above the horizontal wall represents the total flux per unit depth through the branch (and average absolute velocity) at that instant of time. Another horizontal line in the upper left gives the relative magnification of all velocity vectors. The magnification varies from figure to figure because the velocity magnitudes vary considerably through the cycle (recall that $\hat{Re} = 2 Re(S)$ and min $Re = 0$). To reduce them to a common scale, divide the velocity vectors by the relative magnification length. At the time of zero flux ($t' = \pi$) there is considerable backflow near the outer walls of the daughter channel. By the time $t' = \frac{3}{2}\pi$
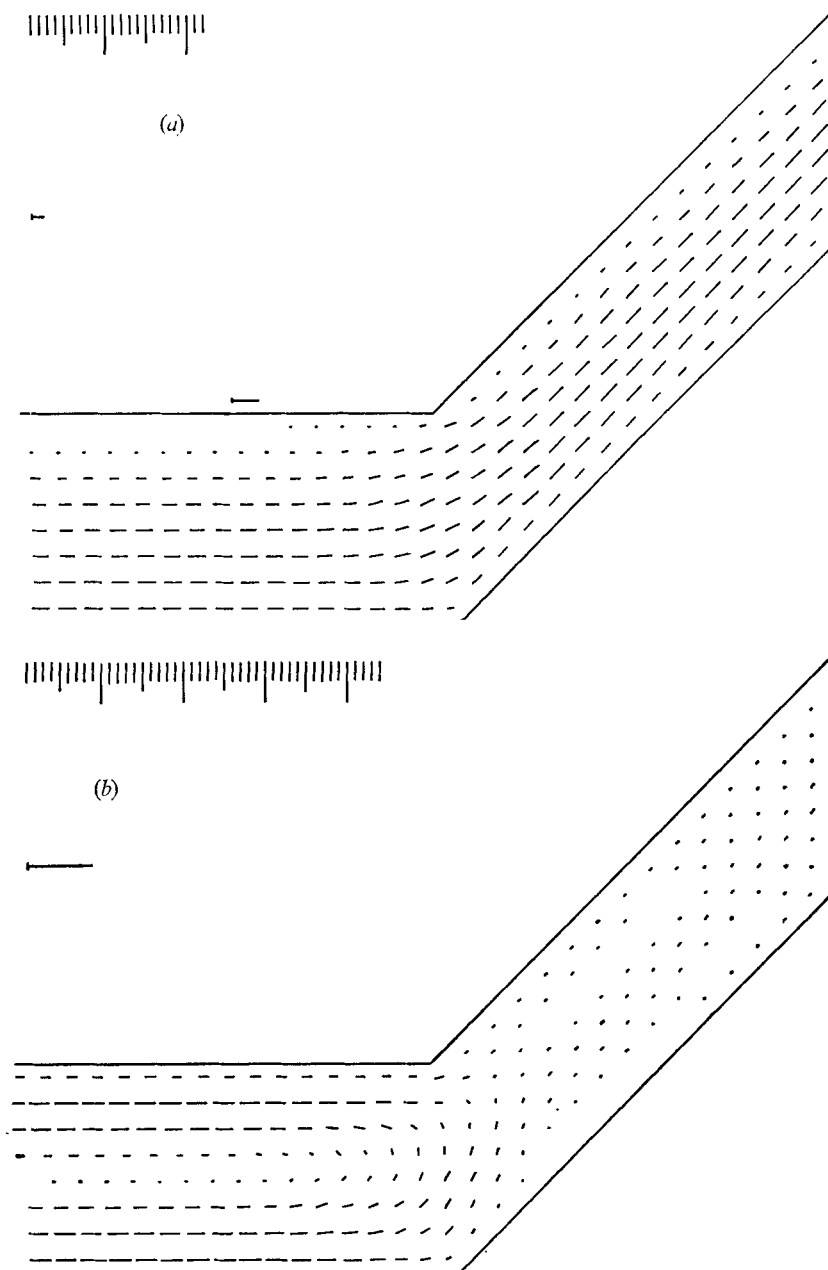
FIGURES 6 (*a*, *b*). For legend see facing page.

(instantaneous flux = mean flux), all flow is forward but the pattern is somewhat different from that when $t' = \frac{1}{2}\pi$ (when again instantaneous flux = mean flux). Near $t' = 0$ or 2π (maximum flux) there are indications of separation from the back of the corner. However, this separation region does not extend very far into the daughter channel, as revealed by close inspection of the stream-function field.
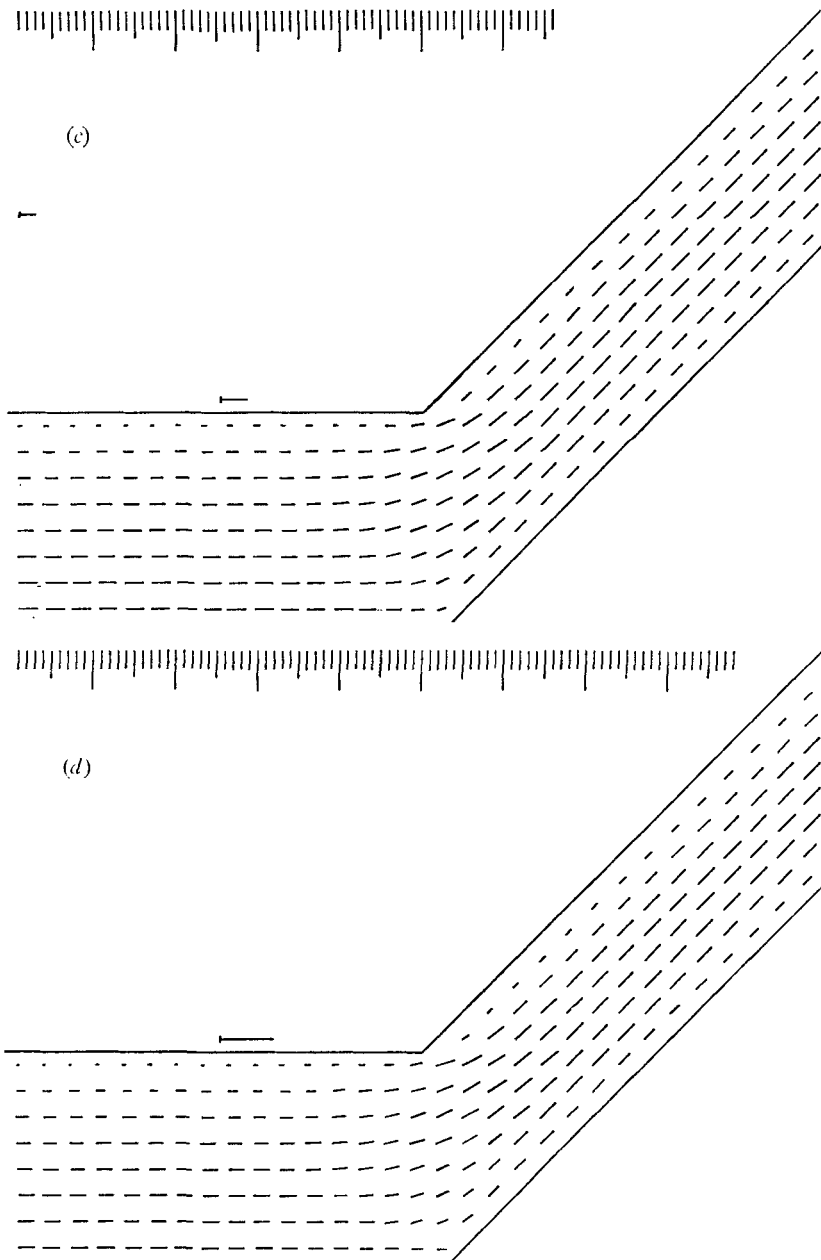
FIGURE 6. Velocity vectors within the branch at four instants during the pulsatile flow cycle ($\hat{R}e = 400$, $N = 10$, $h = \frac{1}{16}$). (a) $t' = \frac{1}{2}\pi$, (b) $t' = \pi$, (c) $t' = \frac{3}{2}\pi$, (d) $t' = 2\pi$.

Because separation and reverse flow are features of the unsteady branch flow, the display of the approximate location of vorticity zeros,† which mark the instantaneous separation and reattachment points on the walls, should be of

† The flow separates or reattaches somewhere close to the indicated curves, but inter-polation for a 'more precise' location was not warranted for the coarse mesh (see appendix).
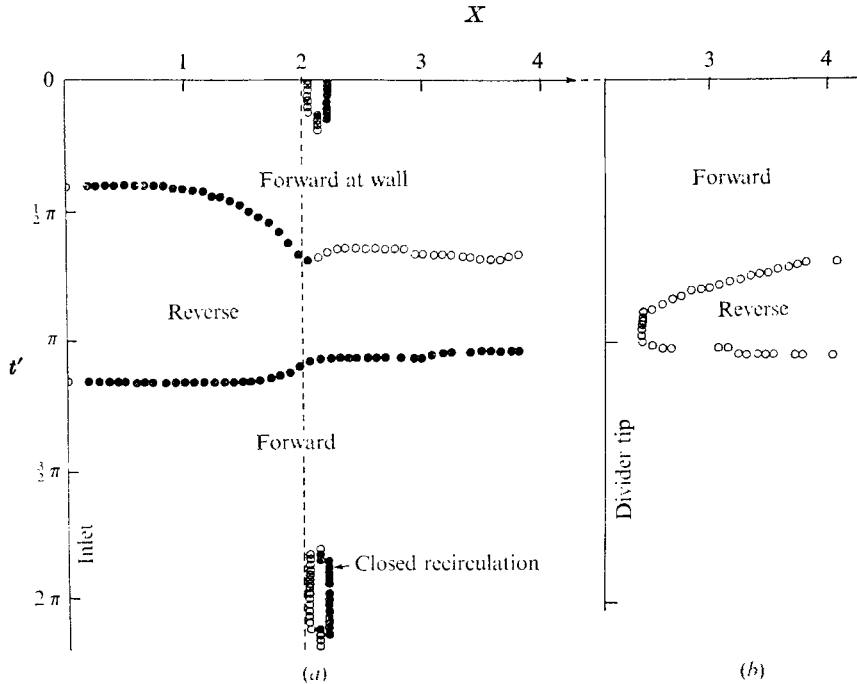
FIGURE 7. Approximate location of separation and reattachment points in the branch during the pulsatile flow cycle. (a) Outer wall. (b) Inner wall. ○, separation; ●, reattachment.

interest (figure 7). During a portion of the cycle there is reverse flow at the walls all along the outer boundary and most of the divider. Only the divider tip does not experience flow reversal. During another portion of the cycle, the flow reattaches to the parent channel walls as it approaches the daughter channels. During yet another part of the cycle, around peak flux time, there is separation and reattachment just beyond the corner ($X = 2$) on the outer wall. The size and duration of this closed circulation region are very sensitive to the mesh size used in the calculation *and* the corner vorticity boundary approximation. Using the approximation most appropriate to a smooth physical boundary gave the most consistent results as $h \to 0$, but the size of the corner circulation region (in space and time) became smaller when h was halved from $\frac{1}{8}$ to $\frac{1}{16}$. The other loci of reattachment and separation were essentially the same at $h = \frac{1}{8}$ and $h = \frac{1}{16}$ (see Friedman *et al.*). No separation was found for the steady flow, $Re(S) = 200$.

The separation phenomenon in the bifurcation differs from that in a diverging channel without flow splitting (Schneck & Ostrach 1973). The effect of the divider is to minimize or prevent transient detachment on the outer wall, as shown in complementary calculations by decreasing the area ratio α from a large value to the one shown here.

In arterial haemodynamics the wall shearing stress is an important dimensional quantity (see Fry 1968), and is directly proportional to the non-dimensional wall vorticity Ω_w: $\tau_w(X, Y, t') = [8\mu^2 Re(S)/\rho(2L)^2] \Omega_w(X, Y, t')$. The distribution of
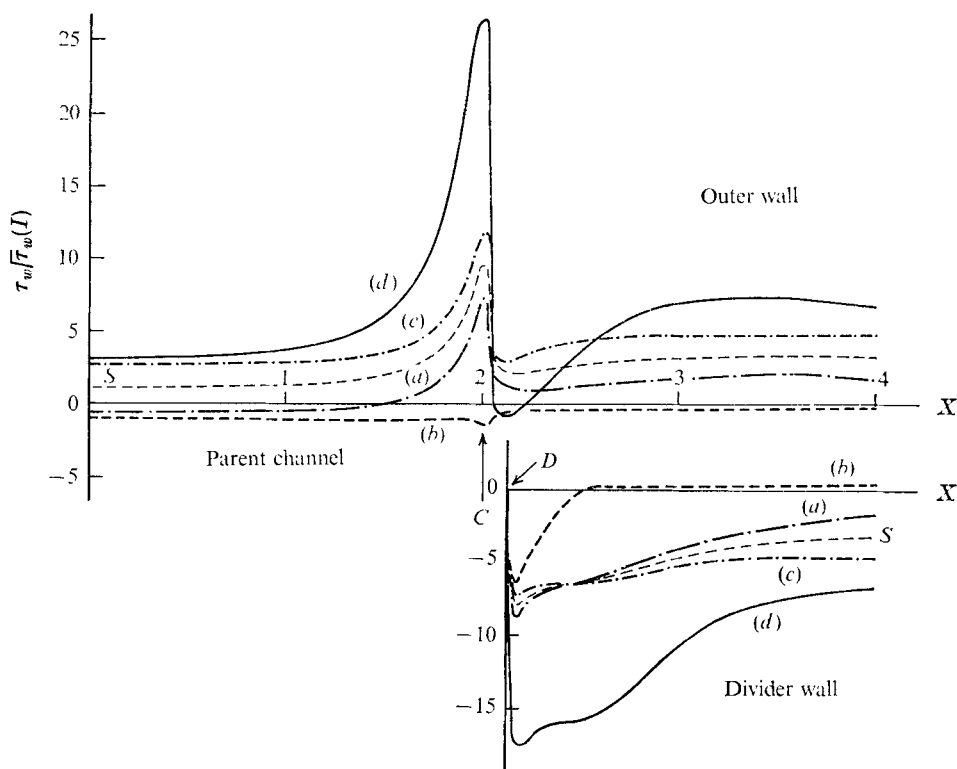
FIGURE 8. Relative wall stress $\tau_w/[\tau_w(I)]$ within the branch at four instants during the pulsatile flow cycle (and S = steady flow). (a) $t' = \frac{1}{2}\pi$ (mean flux). (b) $t' = \pi$ (minimum). (c) $t' + \frac{3}{2}\pi$ (mean). (d) $t' = 2\pi$ (peak).

Ω_w (or τ_w) along the upper bounding walls is shown at four times during the periodic cycle in figure 8.† At $t' = \frac{1}{2}\pi$ (curve (a): instantaneous flux = mean flux), the outer wall vorticity Ω_w rises from its upstream negative value to a high positive value just before the corner, and then falls towards the lower positive downstream daughter channel value. At $t' = \pi$ (curve (b): zero flux), Ω_w is everywhere negative but small. At $t' = \frac{3}{2}\pi$ (curve (c): instantaneous flux = mean flux again), Ω_w rises from a moderate positive value to a much higher value just before the corner, and then with a single oscillation settles down to the downstream channel value. At the end of the cycle, $t' = 2\pi$ (curve (d): peak flux), the wall vorticity (and hence also τ_w) rises to a very high value near the corner C. It falls to a negative value just behind the corner (the recirculation region). Then it gradually approaches the downstream channel value. The corresponding steady stress distribution is also shown. The instantaneous peak wall vorticity, or $\hat{\Omega}_w$, is many times the input peak $\Omega_w(I)$, which is in turn higher than the mean upstream value $\hat{\Omega}_w(S)$. The values plotted are not necessarily quantitatively significant (owing to numerical approximation) but their trend should be.

The distribution of vorticity and stress is also shown for the divider or inner

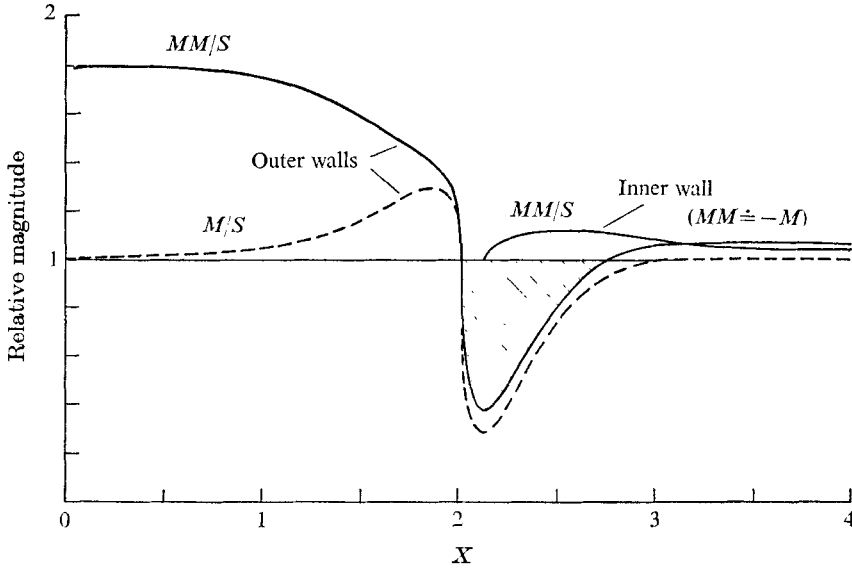† The vorticity has opposite sign on the symmetrical wall in the lower half of the **Y**.

FIGURE 9. Comparison of mean relative stress (M) and mean magnitude relative stress (MM) distributions with the steady relative stress distribution (S).

$$M \equiv \frac{1}{\bar{\tau}_w(I)} \frac{1}{2\pi} \int_0^{2\pi} \tau_w(t')\, dt',$$

$$MM \equiv \frac{1}{\bar{\tau}_w(I)} \frac{1}{2\pi} \int_0^{2\pi} |\tau_w(t')|\, dt',$$

$$S \equiv \tau_w(S)/\bar{\tau}_w(I).$$

wall. There is a sharp initial rise in magnitude and slower decay to the downstream parallel value. The extrema of Ω_w, both peaks and minima, vary along the walls, and their phase relative to the input flux also varies. The mean (time-average) wall vorticity varies with downstream distance and thus the mean wall shearing stress does not equal the steady shearing stress near the junction owing to the nonlinearity of the flow. Since the force on the wall is just as strong for reverse shear as for forward flow, the mean magnitude of τ_w or $\overline{|\tau_w|}$ is perhaps a better indication of the flow-induced wear and tear on wall surfaces. Comparisons with the steady relative stress distribution are shown in figure 9.

Qualitatively quite similar results were obtained for other simple pulsatile flow calculations. The peak values of the shear and its minima vary, the magnitudes increasing with $Re(S)$ increasing, N increasing or α decreasing. The locations of these extrema do not migrate.

In vivo flux wave

The shape of a realistic arterial flux wave was obtained from a catheter probe in the iliac artery of a young boy during the course of an operation; see figure 10 (thanks to Dr L. J. Krovetz, Johns Hopkins Hospital). It was not possible to quantify the flux at the same time, but for comparison purposes it was assumed
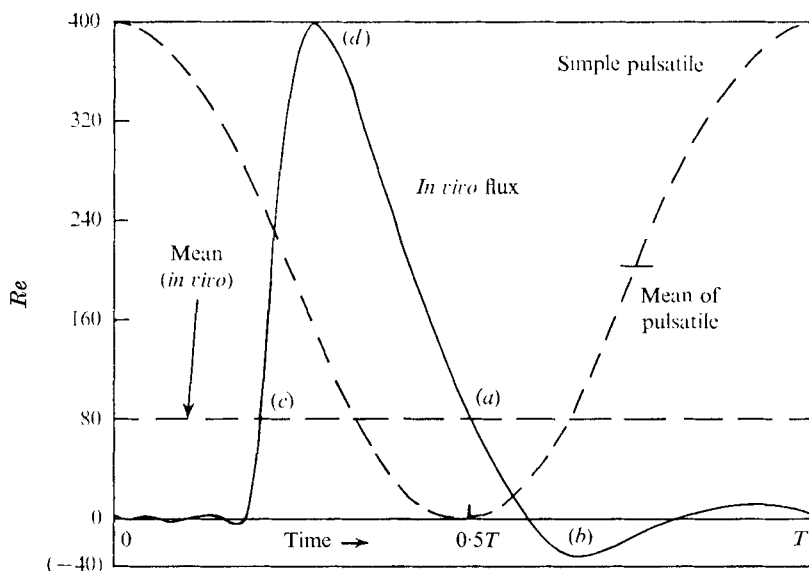
FIGURE 10. Time dependence of human abdominal aortic flux wave; simple
pulsatile wave also shown.

that the peak flux was equal to that in the previous simple pulsatile flow example,
namely $\hat{R}e = 400$ (figure 10). (Quite similar flux waves had been recorded near
the abdominal aortic branches in dogs by previous researchers; see Gutstein,
Farrell & Schneck 1970.) One immediate difference between the real flux wave
and the simple pulsatile one is the peak-to-mean ratio R. For the simpler wave
it was fixed at 2, but the real wave has $R = 5$. (In animals and humans this ratio
is often in the range 3–6.) The simpler wave had a minimum of zero, but the real
wave indicates *negative* net flow during a fraction of the cycle immediately
following the peak pulse (and also some small high frequency oscillations about
zero). The phase difference between the two waves is arbitrary, of course; the
indicated time of the *in vivo* wave is relative to the R-wave of the heart. The
Stokes number N was assigned the same value as in the previous example.

The fully developed velocity profiles as a function of time required for the input
to the numerical program were obtained by a finite-difference solution of the
parallel (one-dimensional) flow equation with the flux wave as a boundary con-
dition. This direct solution is quicker and easier than doing a (numerical) Fourier
analysis in terms of the basic period and then combining the harmonic analytic
solutions. The other boundary conditions for the full two-dimensional calculation
in the bifurcation remain the same (figure 4).

Although the simple pulsatile flux wave and the *in vivo* one were assigned the
same basic similarity parameters, peak Reynolds number $\hat{R}e$ and Stokes number
N, the variation in flux-wave shape obviously creates differences between the
respective unsteady branch flows. The quarter-cycle vorticity (wall stress)
distributions of the simple wave (figure 8) occurred at peak, mean (2) and mini-
mum flux. The corresponding stress distributions at the instants of peak (d),
mean (2) (a and c) and minimum flux (b) for the *in vivo* wave are shown in figure 11.
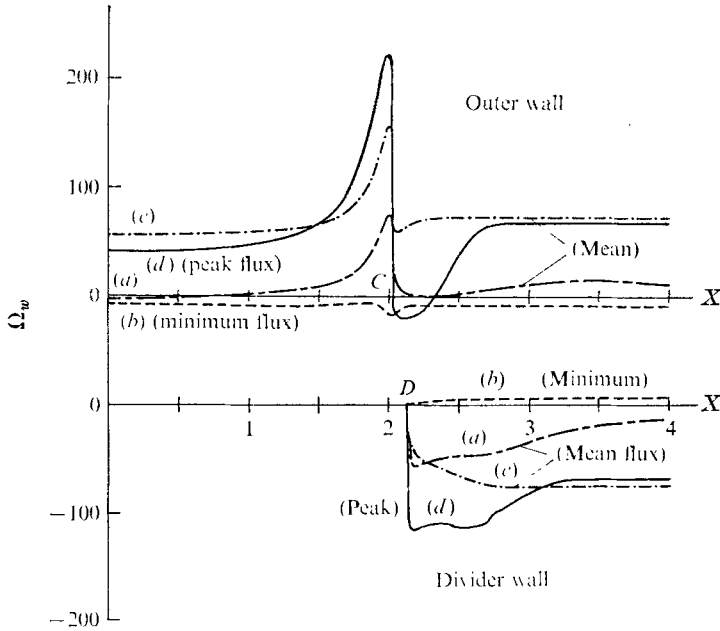
FIGURE 11. Wall vorticity distributions at four instants for *in vivo* flux wave. (a) Mean flux. (b) Minimum flux. (c) Mean flux. (d) Peak flux.
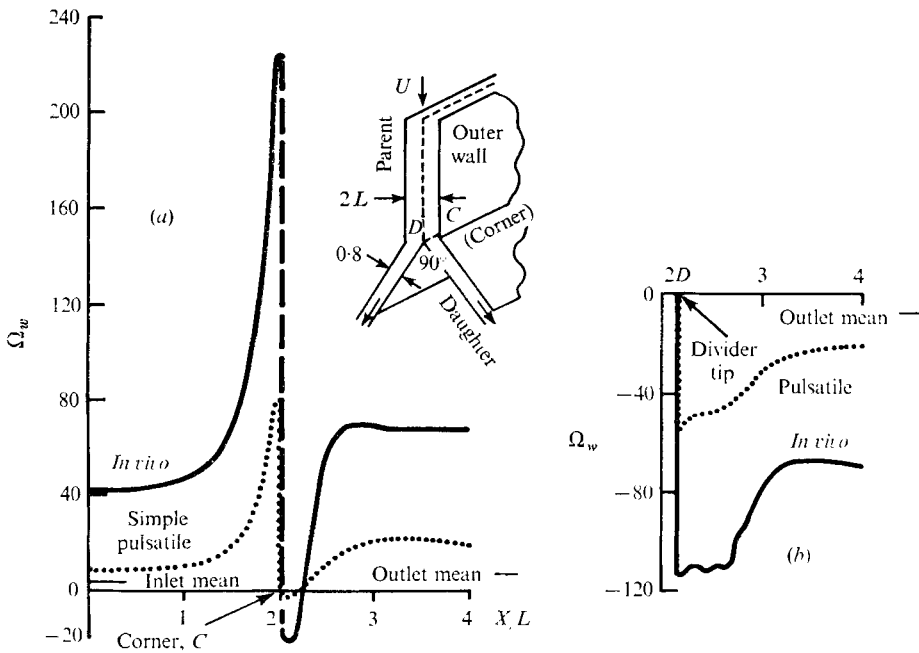

FIGURE 12. Wall vorticity distribution for the *in vivo* wave at peak flux.
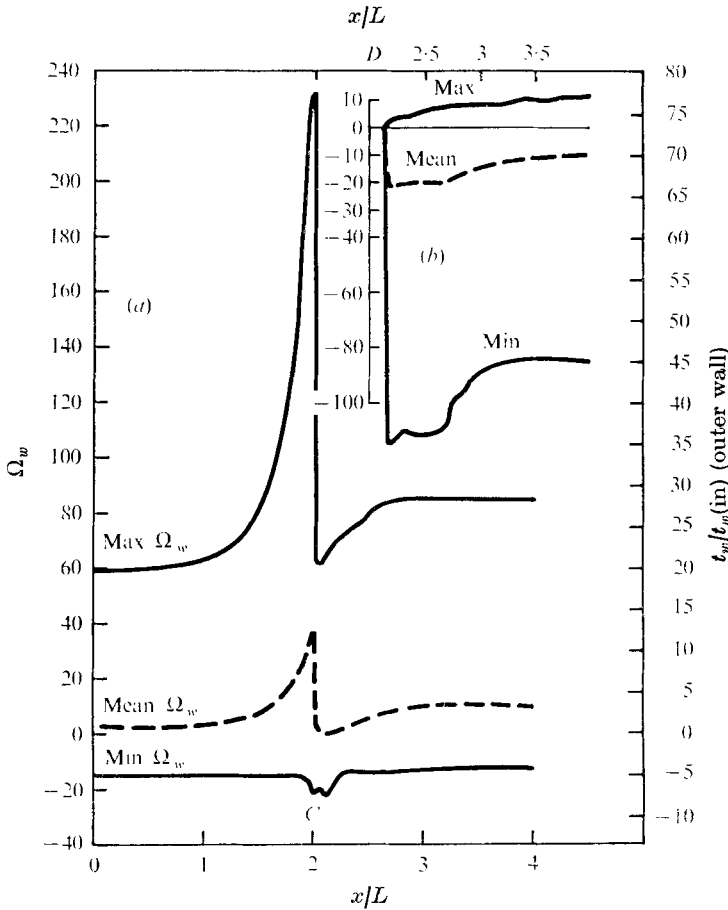
FIGURE 13. Wall vorticity extrema for the *in vivo* wave (compared with mean Ω_w).
(*a*) Outer wall. (*b*) Divider wall.

Of course, only at the instant of peak flux is the net flow through the bifurcation the same for the two flows. The Ω_w distributions at $\hat{R}e$ with the wall vorticity normalized by the mean inlet values are compared in figure 12. Not surprisingly, for the higher R wave the parallel inlet (and also outlet) flow has greater vorticity, but the ratio is higher than $5:2$. This appears to be due to the relatively steep rise of the *in vivo* flux wave to its peak, compared with the simple harmonic one. As with the simpler wave there is a sharp rise in vorticity at the outer corner of the bifurcation, followed by a drop to a negative value just past the corner. The magnitudes of the extrema are greater at larger R. The magnitude of the vorticity distribution near the divider tip is also greater for the larger R. However, the curves are qualitatively similar, indicating that the major changes from the parallel inlet and outlet values lie close within the junction. (The wiggles on the divider-tip distributions may be due to the inadequacy of the fixed mesh calculation to represent accurately the highest harmonics of the flux wave; see appendix.) Extremum values of Ω_w are compared with the mean values in figure 13.
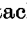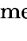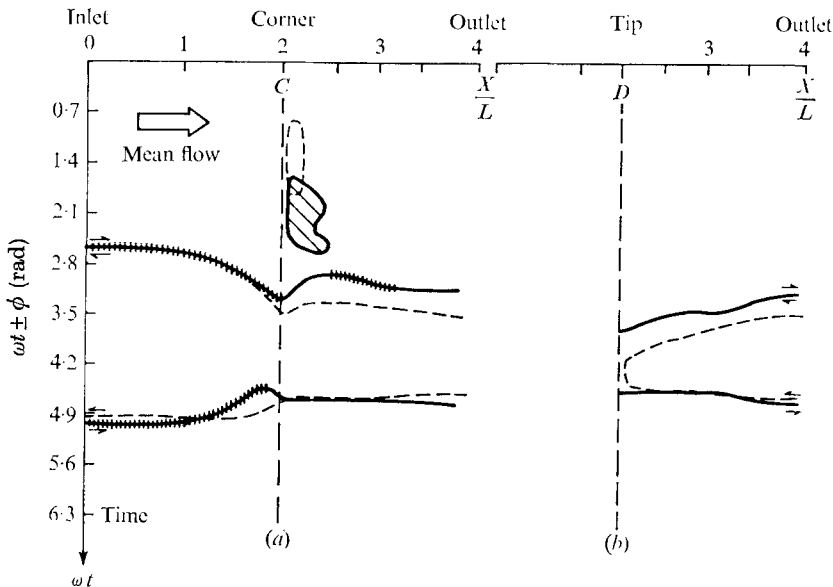
FIGURE 14. *In vivo* separation–reattachment pattern (with simple pulsatile one). (*a*) Outer wall. (*b*) Divider wall. ━━━, reattachment; ——, separation, ▨, closed circulation.

The instantaneous velocity vector patterns for the *in vivo* wave are qualitatively similar to the simple harmonic case at peak and mean flux. At the time of greatest negative flux (minimum flow) all the velocity vectors are directed upstream.

It was expected that the approximately 20 % of the cycle with negative flux, and the more intense flow reversal behind the outer corner, would imply great differences in the separation patterns throughout the cycle. Actually, if the phases of the two flux waves are adjusted such that the times of inlet wall flow reversal coincide, as in figure 14, where the simple pulsatile flow results are dashed, the time–distance variation of the zeros of the vorticity (which mark detachment or reattachment of instantaneous streamlines to the wall) is not very different. The recirculation bubble at the outer corner is longer in length and duration, but only slightly. The separation point on the divider moves forward, right to the tip, moving off as the flux becomes negative. The reattachment to the outer wall after total flow reversal (*in vivo*) is only slightly different from the wall reversal alone (simple pulsatile).

In summary, the distributions of wall vorticity with the *in vivo* wave are rather similar in shape to the simple pulsatile ones regarding the locations of extrema on the outer wall and the divider tip. Only the magnitudes of the vorticity extrema change, increasing with R. The separation patterns on the outer wall are similar; the difference on the divider tip is due to the portion of the cycle having reverse flux.

5. Discussion

The solutions presented here have given an indication of the complexity of unsteady branching flow. Yet they are far from complete as a total picture of pulsing blood flow. Some of the ways in which they are unrealistic are listed below, so that it is clear that the application to arterial haemodynamics is qualitative. However, the potentialities of the numerical technique to predict more closely the actual flow patterns theoretically are also pointed out.

Disadvantages of present model as an arterial one

A major drawback is a topological one: all real branches are three-dimensional. Our two-dimensional model cannot predict the secondary flows which have been observed in branch flows, steady and unsteady (Zeller, Talukder & Lorenz 1970; Brech & Bellhouse 1973). However, if the three-dimensional geometry has another orthogonal plane of symmetry the secondary flow helices go in opposite directions relative to this plane, which means that there is no secondary flow contribution to the wall shear along the plane's intersection with the wall. So there the wall shear distribution will depend on $\hat{R}e$, R and N as in the present examples (neglecting minor variations in flux-wave shape). This has been borne out by experimental measurements in a rectangular duct branch (Bargeron *et al.* 1975).

Real arterial geometries are not of uniform cross-section, nor are corners sharp. The angles of bifurcation vary. Also, arterial junction geometries are not fixed because the elastic walls yield to the unsteady pressure pulses of the flowing blood. In addition, blood is not really a Newtonian fluid, but a viscoelastic suspension of erythrocytes and other elements.

Advantages of numerical theory

As demonstrated within the present bifurcation geometry, it is easy to vary the important dynamic parameters† to assess the dependence of unsteady flow patterns on them. Given the inflow flux, all features of the pulsatile branch flow can be predicted including wall shear and separation patterns. (Perhaps it will be possible to find a correlation between flux-wave shapes and local progress of atherosclerosis.) The velocity fields can be used to calculate the convective terms in mass-transport analyses, which are necessary to describe the coupling between the biochemistry and haemodynamics (Caro *et al.* 1969, 1971).

Similar two-dimensional calculations in rigid branches with non-uniform cross-sections with rounded walls and/or other angles can be performed by means of 'short-leg' finite-difference approximations at the boundaries.

The inclusion of moving boundaries in three dimensions and modelling blood's viscoelastic properties are computational predictive tasks still far in the future. It will be difficult and expensive to do numerically (but nothing else is feasible). The methods to be developed will almost certainly depend upon the availability

† At least up to $\hat{R}e = 400, N = 10$.

of measurements of the pertinent physical properties and the desired accuracy of haemodynamic theoretical predictions.

6. Conclusions

The detailed dynamics of plane pulsatile flows in a two-dimensional bifurcation have been presented. The numerical method is applicable to a wide range of the dynamic parameters, $\hat{R}e$ and N, and flux-wave shape, as well as other two-dimensional geometries. The results show the inability of a steady two-dimensional flow calculation to predict quantitatively even the mean forces developed by such a nonlinear time-dependent flow; they depend upon the shape and magnitude of the flux wave. The unsteady maximum forces are much larger than the mean ones; they depend upon flux-wave shape also.

The numerical calculations definitely indicate local flow differences close within the junction. For both flux waves there are high shearing forces (transient, peak and mean) in the branch. They tend to be localized near the outer wall corner and near the divider tip as in steady flow simulations but exceed the steady values. Unlike steady flow at the same mean Reynolds number, there is also a transient separation bubble just inside the branch on the outer wall. Judging from the bifurcation of an unbounded uniform flow (Kaplan 1966), one could anticipate quantitative lowering of the maximum shearing stress with corner rounding, but the trend of peak ratios and locations probably remains essentially the same. The maxima increase with $Re(S)$, R and N increasing (and also with α decreasing, i.e. smaller branches). There is no doubt that complex branching pulsatile flow patterns affect the convective transport of biologically important substances.

Appendix. Accuracy of numerical nonlinear analysis

The feat of obtaining a numerical nonlinear flow simulation is always tempered by a lack of knowledge of the accuracy of the approximation. Until this section is superseded by complete objective experimental comparison, a discussion is presented to place the present calculations in perspective.

First, the form of the vorticity transport equation (1) differs from another popular one (e.g. Roache 1972, equation 2–12) in two respects. Usually

$$\partial\Omega/\partial t' = -\nabla \cdot (\mathbf{U}'\Omega) + Re^{-1}\nabla^2\Omega;$$

at high Reynolds numbers in steady flows with slight unsteady perturbations, the nonlinear convection dominates the viscous diffusion and $L/\langle U_s \rangle$ is taken as the characteristic time. Roache also uses the so-called 'conservative form' of the convective term, but for incompressible flow the term can be reduced analytically to the form given in (1). It is sometimes claimed that the use of corresponding finite-difference forms of the two convective expressions leads to two different solutions of steady-state problems solved by numerically relaxing an initial transient (e.g. Torrance & Rockett 1969). Close inspection often reveals differences in setting up the problem other than just the convective term. The

stability of an explicit marching scheme obviously can be affected by the form of the convective term, but that question is clouded by the apparent stability variation due to changes in the Ω boundary-value approximation (see Lugt & Rimon 1970; Roache 1972). At any rate, the solutions discussed here were stable for the time steps used in the marching technique.

On the other hand, as in our calculations, Pearson (1965) used a non-conservative nonlinear term and second-order vorticity boundary approximation for numerical calculation of Ψ and Ω in a known exact time-dependent (decay) problem. The comparison of the numerical result with the exact analytic solution (his table 2) was quite reasonable. The actual numerical accuracy will be related to the mesh size h and the convergence criterion for the relaxation iteration.

Our convergence criterion, a residual ϵ of order 10^{-6}, was applied at a point at two times separated by 2π. After the solution had converged, a final cycle checked the absolute relative errors per cycle of Ψ, Ω, Ψ_x and Ψ_y at each mesh point. In general these were of order 10^{-4}, the largest errors, of order 10^{-3}, occurring only near the points where the variable changed sign.

As the size of a finite-difference mesh decreases, the finite-difference approximation theoretically approaches the solution of the continuum governing equations. The difference is sometimes called 'truncation convergence' to distinguish it from the iteration convergence above. For oscillatory flow there is a natural 'viscous length', $O(\nu/\omega)^{\frac{1}{2}}$, so that adequate representation of the unsteady flow requires $h \ll \sqrt{2}/N$. There were irregularities in the large ($\frac{1}{8}$) mesh field solution, which were ironed out when the mesh was reduced to $\frac{1}{16}$ for the wall vorticity approximation described above (including the corner one).

The mathematical 'dilemma' of flow singularities near a sharp convex corner has received considerable attention in the literature of elliptic and quasi-elliptic equations (Fox 1971; Walsh 1971; Birkhoff 1972). A mathematically sharp corner is physically unrealistic for any continuum flow. The corner here is regarded as smoothed off symmetrically to a small radius of curvature ($\ll h$). Then the corner normal is effectively along the bisector and the present numerical approximation of vorticity is appropriate and convenient.

Surprisingly, varying *just* the convex-corner vorticity approximation had a relatively large effect on the local flow solution. The time-dependent separation region was quite different for large and small meshes with a number of other popular vorticity approximations at the corner. This finding for the unsteady flow is rather similar to others' experience with convex corners in steady viscous flow fields (Stevenson 1972; Lugt & Haussling 1972; Underwood & Mueller 1972). The second-order average normal has been shown to be more consistent with analytical theoretical expectations for steady Stokes flow ($Re \to 0$) and the numerical solutions showed less variability as the mesh size decreased ($h \to 0$). Separation from a point close to the corner was involved in these calculations, just as sometimes occurs here in the pulsatile flow solutions in the branch. Very fine mesh solutions are required to present accurately the details of the separation phenomenon near corners. (See also Mozayeny 1970.)

Unsteady numerically calculated separation on a stationary flat wall must pass the same stringent 'regularity test' which exists (but is not generally acknow-

ledged) for steady separation accuracy. From the analyses of Dean (1950) and Oswatitsch (1958) the three main points of the regularity test for a flat wall are as follows.

(i) The separation (or attachment) streamline and the zero-vorticity contour intersect the wall at the same location.

(ii) The slopes of the separation streamline and the zero-vorticity contour have the same sign at the wall.

(iii) These slopes are in the exact ratio 3:1.

Applying this test to our finer mesh ($\frac{1}{16}$) calculated results for separation on the flat divider wall (where the separation phenomenon is not confused with the corner) reveals the following.

(i) The interpolated wall intersections of the separation streamline and the zero-vorticity contour are at nearly the same location (within a mesh length) except when the location is changing rapidly with time.

(ii) Even though the locations may differ, the slopes at the wall do have the same sign.

(iii) For a particular case (zero flux) (figure 15) where the locations do coincide (within the error of the calculation) the slopes are approximately in the ratio 3:1.

The calculation passes the regularity test qualitatively if not quantitatively. It should be noted that nearly all published nonlinear numerical analyses would get low grades on this test, but it has seldom been applied. A solitary author (Leal 1973) mentions its existence and his steady computation reasonably satisfies (i) and (ii) but fails (iii).

Finally, the outlet flow is forced to be parallel to the daughter walls. The numerically computed parallel flow there can be compared with the analytic fully developed time-dependent solution. The question of accuracy should consider whether the downstream boundary condition has been imposed too close to the junction. The asymptotic approach to fully developed parallel flow depends upon the Reynolds number in general and a fixed downstream boundary will cease to be appropriate at some Re for the pulsatile inlet flow. The outlet at $X = 4$ seems all right for the steady flow alone, $Re(S) = 200$, because the calculated outlet vorticity is linear to a very good approximation. Also the centre-line velocity differs less than 1% from the analytic one, a practical criterion often used to define 'fully developed'. However, there are indications, such as small asymmetries, that the downstream boundary at $X = 4$ is barely far enough for the exit flow to become parallel when $Re = 400$, even though the mean wall shear and mean centre-line velocity are within 1% of the analytic values. A doubling of the inlet and outlet lengths produced the anticipated small changes in the calculated values within the junction and showed better agreement with the expected developed flow at the outlet location.
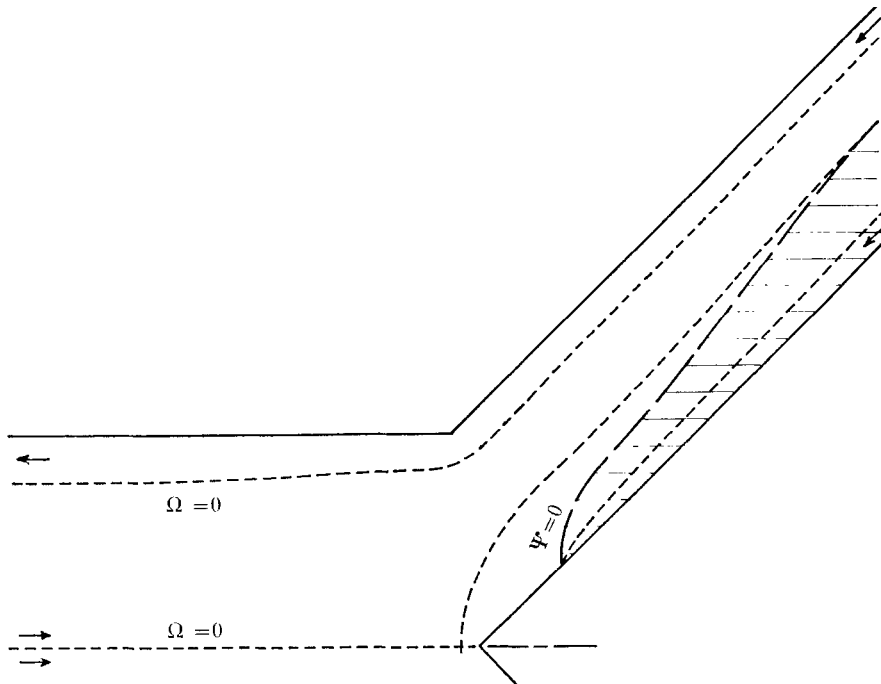
FIGURE 15. Separation streamline ($\Psi = 0$) and zero-vorticity contours ($\Omega = 0$) for $t' = \pi$ or $t = 0.5T$ (see figures 6(b) and 8(b)).

REFERENCES

BARGERON, C. B., MARK, F. F. & FRIEDMAN, M. H. 1975 *28th Ann. Conf. Engng Med. Biol.*, paper D5.12.

BIRKHOFF, G. 1972 *J. Approx. Theor.* **6**, 215.

BRECH, R. & BELLHOUSE, B. J. 1973 *Cardiovasc. Res.* **7**, 593.

BUZBEE, B. L., DORR, F. W., GEORGE, J. A. & GOLUB, G. H. 1971 *SIAM J. Numer. Anal.* **8**, 722.

CARO, C. G., FITZ-GERALD, J. M. & SCHROTER, R. C. 1969 *Nature*, **223**, 1159.

CARO, C. G., FITZ-GERALD, J. M. & SCHROTER, R. C. 1971 *Proc. Roy. Soc.* B**177**, 109.

CHENG, T. S. & FIJAS, D. F. 1972 *Bull. Am. Phys. Soc.* **17**, 1115.

CLARK, M. E. & ROBERTSON, J. M. 1971 *24th Ann. Conf. Engng Med. Biol.*, paper 16.4.

CONSTANTINIDES, P. 1965 *Experimental Atherosclerosis.* Elsevier.

DEAN, W. R. 1950 *Proc. Camb. Phil. Soc.* **46**, 293.

DOWNIE, H. G., MUSTARD, J. F. & ROWSELL, H. C. 1963 *Ann. N.Y. Acad. Sci.* **104**, 539.

EHRLICH, L. W. 1971*a* *SIAM J. Numer. Anal.* **8**, 278.

EHRLICH, L. W. 1971*b* *Appl. Phys. Lab., Johns Hopkins Univ. Rep.* TG-1169.

EHRLICH, L. W. 1973*a* *Appl. Phys. Lab. Johns Hopkins Univ. Rep.* TG-1218.

EHRLICH, L. W. 1973*b* *Appl. Phys. Lab. Johns Hopkins Univ. Rep.* TG-1219.

EHRLICH, L. W. 1974 *Comp. & Fluids*, **2**, 237.

FOX, J. A. & HUGH, A. E. 1966 *Br. Heart J.* **28**, 388.

FOX, L. 1971 *Proc. Roy. Soc.* A**323**, 179.

FRIEDMAN, M. H., O'BRIEN, V. & EHRLICH, L. W. 1975 *Circ. Res.* **36**, 277.

FRY, D. L. 1968 *Circ. Res.* **22**, 165.

GEISSINGER, H. D., MUSTARD, J. F. & ROWSELL, H. C. 1962 *Can. Med. Ass. J.* **87**, 405.

GEORGE, J. A. 1970 *Stanford Univ. Rep.* STAN-CS-70-159.

GOSLING, H. & SEGRE, McK. 1969 *J. Atheroscler. Res.* **9**, 47.

GRACE, S. F. 1928 *Phil. Mag.* **5**, 933.

GUTSTEIN, W. H., FARRELL, G. A. & SCHNECK, D. J. 1970 *Atheroscler.* **11**, 485.

HAUST, M. D. 1971 In *The Artery and the Process of Arteriosclerosis*, p. 272. Plenum.

HOCKNEY, R. W. 1965 *Ass. Comp. Machinery J.* **12**, 95.

HUNG, T. K. & NAFF, S. A. 1969 *8th Int. Conf. Med. Biol. Engng.*

KAPLAN, C. 1966 On the flow of an Oseen-like fluid past a parabolic cylinder. *Air Force Office Sci. Res. Rep.* AFOSR-66-001.

KHAMRUI, S. R. 1957 *Bull. Calcutta Math. Soc.* **49**, 57.

LEAL, L. G. 1973 *J. Fluid Mech.* **59**, 513.

LUGT, H. J. & HAUSSLING, H. J. 1972 *Naval Ship R. & D. Center Rep.* no. 3748.

LUGT, H. J. & RIMON, Y. 1970 *Naval Ship R. & D. Center Rep.* no. 3306.

LYNN, N. S., FOX, V. G. & ROSS, L. W. 1972 *Biorheol.* **9**, 61.

MIDDLEMAN, S. 1972 *Transport Phenomena in the Cardiovascular System*, chap. 2. Interscience.

MOZAYENY, B. 1970 Ph.D. thesis, University of Minnesota.

MURPHY, E. A., ROWSELL, H. C., DOWNIE, H. G., ROBINSON, G. A. & MUSTARD, J. F. 1962 *Can. Med. Ass. J.* **87**, 259.

MUSTARD, J. F., MURPHY, E. A., ROWSELL, H. C. & DOWNIE, H. G. 1964 *J. Atheroscler. Res.* **4**, 7.

O'BRIEN, V. 1975 *J. Franklin Inst.* **300**, 225.

O'BRIEN, V. & LOGAN, F. E. 1966 *Phys. Fluids*, **9**, 214.

OSWATITSCH, K. 1958 *IUTAM 1957 Symp. Grenzschichtforschung*, p. 357. Springer.

PEARSON, C. E. 1965 *J. Fluid Mech.* **21**, 611.

ROACHE, P. J. 1972 *Computational Fluid Dynamics*, chap. 3. Hermosa.

ROTT, N. 1964 In *Theory of Laminar Flows*, p. 401. Princeton University Press.

SCHNECK, D. J. & OSTRACH, S. 1973 *Case Western Reserve Univ. Rep.* FTAS/TR-73-86.

SEXL, T. 1930 *Z. Phys.* **61**, 349.

SPENCER, M. P. & DENISON, A. B. 1963 In *Handbook of Physiology*, vol. 11. *Circulation*, p. 839. Am. Physiol. Soc.

STEVENSON, J. F. 1972 *Trans. A.S.M.E.* E**93**, 355.

TEXON, M., IMPARATO, A. M. & HELPERN, J. 1965 *J. Am. Med. Ass.* **194**, 168.

TEXON, M., IMPARATO, A. M. & LORD, J. W. 1960 *Arch. Surg.* **80**, 47.

TORRANCE, K. E. & ROCKETT, J. A. 1969 *J. Fluid Mech.* **36**, 33.

UNDERWOOD, F. N. & MUELLER, T. J. 1972 *25th Ann. Conf. Engng Med. Biol.* paper 34.3.

WALSH, J. 1971 *Proc. Roy. Soc.* A **323**, 155.

WHITMORE, R. L. 1968 *Rheology of the Circulation*, table 7.4. Pergamon.

ZELLER, H., TALUKDER, N. & LORENZ, J. 1970 *Fluid Dynamics of Blood Circulation and Respiratory Flow.* AGARD Conf. no. 65.